An Evaluation of Computational Imaging Techniques for Heterogeneous Inverse Scattering: Supplementary Material

Ioannis Gkioulekas[1], Anat Levin[2], Todd Zickler[1]

[1]Harvard University [2]Weizmann Institute of Science

1 Relationship between time-dependent and stationary RTE

Our analysis in the main paper is based on the time-dependent radiative transfer equation, which we reproduce here for easier reference,

$$\frac{1}{c}\frac{\partial L\left(\boldsymbol{x},\boldsymbol{\omega},t\right)}{\partial t}+\boldsymbol{\omega}\cdot\nabla L\left(\boldsymbol{x},\boldsymbol{\omega},t\right)=-\sigma_t\left(\boldsymbol{x}\right)L\left(\boldsymbol{x},\boldsymbol{\omega},t\right)+\sigma_s\left(\boldsymbol{x}\right)\int_{\mathbb{S}^2}f_p\left(\boldsymbol{x},\boldsymbol{\omega}\cdot\boldsymbol{\psi}\right)L\left(\boldsymbol{x},\boldsymbol{\psi},t\right)\,\mathrm{d}\boldsymbol{\psi},\quad(1)$$

In the computer vision and graphics literature, more commonly encountered is the *stationary* version of the RTE

$$\boldsymbol{\omega}\cdot\nabla L\left(\boldsymbol{x},\boldsymbol{\omega}\right)=-\sigma_t\left(\boldsymbol{x}\right)L\left(\boldsymbol{x},\boldsymbol{\omega}\right)+\sigma_s\left(\boldsymbol{x}\right)\int_{\mathbb{S}^2}f_p\left(\boldsymbol{x},\boldsymbol{\omega}\cdot\boldsymbol{\psi}\right)L\left(\boldsymbol{x},\boldsymbol{\psi}\right)\,\mathrm{d}\boldsymbol{\psi},\quad(2)$$

where, compared to the time-dependent version, L is time-independent and there is no partial derivative with respect to time. This corresponds to the case where the light sources are constant over time, or change very slowly relative to the speed of light.

We can define a Green's function $\mathcal{T}_m^s\left(\boldsymbol{X}_o,\boldsymbol{X}_i\right)$ for the stationary case exactly analogously the time-dependent case. As Equation (1) is linear and shift-invariant with respect to time, we expect that

$$\mathcal{T}_m^s\left(\boldsymbol{X}_o,\boldsymbol{X}_i\right)=\int_0^\infty\mathcal{T}_m\left(\boldsymbol{X}_o,\boldsymbol{X}_i,\tau\right)\,\mathrm{d}\tau.\quad(3)$$

This relationship is often assumed in the literature [4, 1, 3]; we provide an exact statement and formal proof in Proposition 1 below. Equation (3) allows us to interpret the pathlength-resolved Green's function $\mathcal{T}_m\left(\boldsymbol{X}_o,\boldsymbol{X}_i,\tau\right)$ in two equivalent ways: First, $\mathcal{T}_m$ describes the temporal propagation of a pulse of light of infinitesimal duration through the scattering medium. Second, $\mathcal{T}_m$ decomposes $\mathcal{T}_m^s$ into components, each corresponding only to photons that travel a specific pathlength τ inside the medium.

Proposition 1. *Let $L(\boldsymbol{x},\boldsymbol{\omega},t)$ be the solution to the time-dependent RTE*

$$\frac{1}{c}\frac{\partial L(\boldsymbol{x},\boldsymbol{\omega},t)}{\partial t}+\boldsymbol{\omega}\cdot\nabla L(\boldsymbol{x},\boldsymbol{\omega},t)=-\sigma_t(\boldsymbol{x})L(\boldsymbol{x},\boldsymbol{\omega},t)+\sigma_s(\boldsymbol{x})\int_{\mathbb{S}^2}f_p(\boldsymbol{x},\boldsymbol{\omega}\cdot\boldsymbol{\psi})L(\boldsymbol{x},\boldsymbol{\psi},t)\,\mathrm{d}\boldsymbol{\psi}, \quad (4)$$

subject to boundary conditions

$$L(\boldsymbol{x},\boldsymbol{\omega},t)=g(\boldsymbol{x},\boldsymbol{\omega})\delta(t), \qquad (\boldsymbol{x},\boldsymbol{\omega})\in\Gamma_i, \quad (5)$$
$$L(\boldsymbol{x},\boldsymbol{\omega},t)=0, \qquad (\boldsymbol{x},\boldsymbol{\omega})\in(\mathcal{M}\times\mathbb{S}^2)\setminus\Gamma_i, t=0, \quad (6)$$
$$L(\boldsymbol{x},\boldsymbol{\omega},t)=0, \qquad (\boldsymbol{x},\boldsymbol{\omega})\in(\mathcal{M}\times\mathbb{S}^2), t<0. \quad (7)$$

Let $L^s(\boldsymbol{x},\boldsymbol{\omega})$ be the solution to the stationary RTE

$$\boldsymbol{\omega}\cdot\nabla L^s(\boldsymbol{x},\boldsymbol{\omega})=-\sigma_t(\boldsymbol{x})L^s(\boldsymbol{x},\boldsymbol{\omega})+\sigma_s(\boldsymbol{x})\int_{\mathbb{S}^2}f_p(\boldsymbol{x},\boldsymbol{\omega}\cdot\boldsymbol{\psi})L^s(\boldsymbol{x},\boldsymbol{\psi})\,\mathrm{d}\boldsymbol{\psi}, \quad (8)$$

subject to boundary conditions

$$L^s(\boldsymbol{x},\boldsymbol{\omega},t)=g(\boldsymbol{x},\boldsymbol{\omega}), \qquad (\boldsymbol{x},\boldsymbol{\omega})\in\Gamma_i. \quad (9)$$

Then,

$$L^s(\boldsymbol{x},\boldsymbol{\omega})=\int_0^\infty L(\boldsymbol{x},\boldsymbol{\omega},t)\,\mathrm{d}t. \quad (10)$$

Proof. Let $\tilde{L}(\boldsymbol{x},\boldsymbol{\omega},s)=\mathcal{L}\{L(\boldsymbol{x},\boldsymbol{\omega},t)\}$ be the Laplace transform of $L(\boldsymbol{x},\boldsymbol{\omega},t)$ with respect to time. Applying the Laplace transform to Equation (4), it becomes

$$\frac{s}{c}\tilde{L}(\boldsymbol{x},\boldsymbol{\omega},s)+\boldsymbol{\omega}\cdot\nabla\tilde{L}(\boldsymbol{x},\boldsymbol{\omega},s)=-\sigma_t(\boldsymbol{x})\tilde{L}(\boldsymbol{x},\boldsymbol{\omega},s)+\sigma_s(\boldsymbol{x})\int_{\mathbb{S}^2}f_p(\boldsymbol{x},\boldsymbol{\omega}\cdot\boldsymbol{\psi})\tilde{L}(\boldsymbol{x},\boldsymbol{\psi},s)\,\mathrm{d}\boldsymbol{\psi}. \quad (11)$$

If we define

$$\tilde{\sigma}_a(\boldsymbol{x},s)=\sigma_a(\boldsymbol{x})+\frac{s}{c}, \quad (12)$$
$$\tilde{\sigma}_t(\boldsymbol{x},s)=\sigma_s(\boldsymbol{x})+\tilde{\sigma}_a(\boldsymbol{x},s), \quad (13)$$

then we can rearrange the terms in Equation (11) to bring it in a form analogous to the stationary RTE (8),

$$\boldsymbol{\omega}\cdot\nabla\tilde{L}(\boldsymbol{x},\boldsymbol{\omega},s)=-\tilde{\sigma}_t(\boldsymbol{x},s)\tilde{L}(\boldsymbol{x},\boldsymbol{\omega},s)+\sigma_s(\boldsymbol{x})\int_{\mathbb{S}^2}f_p(\boldsymbol{x},\boldsymbol{\omega}\cdot\boldsymbol{\psi})\tilde{L}(\boldsymbol{x},\boldsymbol{\psi},s)\,\mathrm{d}\boldsymbol{\psi}. \quad (14)$$

The stationary RTE (8) can be rewritten equivalently into an integral equation known as the *volume rendering equation* [2],

$$\begin{aligned} L^s(\boldsymbol{x},\boldsymbol{\omega}) =& a(\boldsymbol{x},\boldsymbol{x}_{\partial\mathcal{M}}(\boldsymbol{x},\boldsymbol{\omega}))\, g(\boldsymbol{x}_{\partial\mathcal{M}}(\boldsymbol{x},\boldsymbol{\omega}),\boldsymbol{\omega}) \\ &+ \int_0^{r_{\partial\mathcal{M}}(\boldsymbol{x},\boldsymbol{\omega})} a(\boldsymbol{x},\boldsymbol{x}-r'\boldsymbol{\omega})\,\sigma_s(\boldsymbol{x}-r'\boldsymbol{\omega}) \\ &\int_{\mathbb{S}^2} f_p(\boldsymbol{x}-r'\boldsymbol{\omega},\boldsymbol{\omega}\cdot\boldsymbol{\psi})\, L^s(\boldsymbol{x}-r'\boldsymbol{\omega},\boldsymbol{\psi})\,\mathrm{d}\boldsymbol{\psi}\,\mathrm{d}r'. \end{aligned} \tag{15}$$

where for each point $\boldsymbol{x}\in\mathcal{S}$ and direction $\boldsymbol{\omega}\in\mathbb{S}^2$, we denote

$$r_{\partial\mathcal{M}}(\boldsymbol{x},\boldsymbol{\omega}) = \min\{r : \boldsymbol{x}-r\boldsymbol{\omega}\in\partial\mathcal{M}\}, \tag{16}$$

$$\boldsymbol{x}_{\partial\mathcal{M}}(\boldsymbol{x},\boldsymbol{\omega}) = \boldsymbol{x} - r_{\partial\mathcal{M}}(\boldsymbol{x},\boldsymbol{\omega})\,\boldsymbol{\omega}, \tag{17}$$

and where $a(\boldsymbol{x},\boldsymbol{y})$ is volumetric attenuation along the line segment connecting $\boldsymbol{x},\boldsymbol{y}\in\mathcal{M}$,

$$a(\boldsymbol{x},\boldsymbol{y}) = \exp\left(-\int_0^{\|\boldsymbol{x}-\boldsymbol{y}\|}\sigma_t\left(\boldsymbol{x}-r\boldsymbol{\omega}\left(\boldsymbol{y}\xrightarrow{h}\boldsymbol{x}\right)\right)\,\mathrm{d}r\right). \tag{18}$$

We can similarly rewrite Equation (14) into the following equivalent integral form,

$$\begin{aligned} \tilde{L}(\boldsymbol{x},\boldsymbol{\omega},s) =& \tilde{a}(\boldsymbol{x},\boldsymbol{x}_{\partial\mathcal{M}}(\boldsymbol{x},\boldsymbol{\omega}),s)\,\tilde{L}(\boldsymbol{x}_{\partial\mathcal{M}}(\boldsymbol{x},\boldsymbol{\omega}),\boldsymbol{\omega},s) \\ &+ \int_0^{r_{\partial\mathcal{M}}(\boldsymbol{x},\boldsymbol{\omega})} \tilde{a}(\boldsymbol{x},\boldsymbol{x}-r'\boldsymbol{\omega},s)\,\sigma_s(\boldsymbol{x}-r'\boldsymbol{\omega}) \\ &\int_{\mathbb{S}^2} f_p(\boldsymbol{x}-r'\boldsymbol{\omega},\boldsymbol{\omega}\cdot\boldsymbol{\psi})\,\tilde{L}(\boldsymbol{x}-r'\boldsymbol{\omega},\boldsymbol{\psi},s)\,\mathrm{d}\boldsymbol{\psi}\,\mathrm{d}r'. \end{aligned} \tag{19}$$

In Equation (19), we have

$$\tilde{a}(\boldsymbol{x},\boldsymbol{y},s) = \exp\left(-\int_0^{\|\boldsymbol{x}-\boldsymbol{y}\|}\tilde{\sigma}_t\left(\boldsymbol{x}-r\boldsymbol{\omega}\left(\boldsymbol{y}\xrightarrow{h}\boldsymbol{x}\right),s\right)\,\mathrm{d}r\right), \tag{20}$$

and using Equations (13) and (18),

$$\tilde{a}(\boldsymbol{x},\boldsymbol{y},s) = \exp\left(-\frac{s}{c}\|\boldsymbol{x}-\boldsymbol{y}\|\right)a(\boldsymbol{x},\boldsymbol{y}). \tag{21}$$

Using Equation (21), we can rewrite (19) as

$$\begin{aligned} \tilde{L}(\boldsymbol{x},\boldsymbol{\omega},s) =& \exp\left(-\frac{s}{c}r_{\partial\mathcal{M}}(\boldsymbol{x},\boldsymbol{\omega})\right)a(\boldsymbol{x},\boldsymbol{x}_{\partial\mathcal{M}}(\boldsymbol{x},\boldsymbol{\omega}))\,\tilde{L}(\boldsymbol{x}_{\partial\mathcal{M}}(\boldsymbol{x},\boldsymbol{\omega}),\boldsymbol{\omega},s) \\ &+ \int_0^{r_{\partial\mathcal{M}}(\boldsymbol{x},\boldsymbol{\omega})} \exp\left(-\frac{s}{c}r'\right)a(\boldsymbol{x},\boldsymbol{x}-r'\boldsymbol{\omega})\,\sigma_s(\boldsymbol{x}-r'\boldsymbol{\omega}) \\ &\int_{\mathbb{S}^2} f_p(\boldsymbol{x}-r'\boldsymbol{\omega},\boldsymbol{\omega}\cdot\boldsymbol{\psi})\,\tilde{L}(\boldsymbol{x}-r'\boldsymbol{\omega},\boldsymbol{\psi},s)\,\mathrm{d}\boldsymbol{\psi}\,\mathrm{d}r'. \end{aligned} \tag{22}$$

From the properties of the Laplace transform, we have that for any function $f(t)$,

$$\mathcal{L}^{-1}\left\{\exp\left(-\frac{s}{c}r\right)f(s)\right\} = f\left(t-\frac{r}{c}\right). \tag{23}$$

Applying the inverse Laplace transform to Equation (22), and using the property of Equation (23) and the boundary condition (5), we have

$$\begin{aligned} L(\boldsymbol{x},\boldsymbol{\omega},t) =& a\left(\boldsymbol{x},\boldsymbol{x}_{\partial\mathcal{M}}(\boldsymbol{x},\boldsymbol{\omega})\right) g\left(\boldsymbol{x}_{\partial\mathcal{M}}(\boldsymbol{x},\boldsymbol{\omega}),\boldsymbol{\omega}\right) \delta\left(t-\frac{r_{\partial\mathcal{M}}(\boldsymbol{x},\boldsymbol{\omega})}{c}\right) \\ &+ \int_0^{r_{\partial\mathcal{M}}(\boldsymbol{x},\boldsymbol{\omega})} a\left(\boldsymbol{x},\boldsymbol{x}-r'\boldsymbol{\omega}\right)\sigma_s\left(\boldsymbol{x}-r'\boldsymbol{\omega}\right) \\ &\int_{\mathbb{S}^2} f_p\left(\boldsymbol{x}-r'\boldsymbol{\omega},\boldsymbol{\omega}\cdot\boldsymbol{\psi}\right) L\left(\boldsymbol{x}-r'\boldsymbol{\omega},\boldsymbol{\psi},t-\frac{r'}{c}\right)\,\mathrm{d}\boldsymbol{\psi}\,\mathrm{d}r'. \end{aligned} \tag{24}$$

Finally, let

$$G(\boldsymbol{x},\boldsymbol{\omega}) = \int_0^\infty L(\boldsymbol{x},\boldsymbol{\omega},t)\,\mathrm{d}t. \tag{25}$$

Using the boundary condition of Equation (7), we have

$$\int_0^\infty L\left(\boldsymbol{x},\boldsymbol{\omega},t-\frac{r}{c}\right)\mathrm{d}t = G(\boldsymbol{x},\boldsymbol{\omega}), r \geq 0. \tag{26}$$

Then, integrating both sides of Equation (24) over time and using equation (26), we have

$$\begin{aligned} G(\boldsymbol{x},\boldsymbol{\omega}) =& a\left(\boldsymbol{x},\boldsymbol{x}_{\partial\mathcal{M}}(\boldsymbol{x},\boldsymbol{\omega})\right) g\left(\boldsymbol{x}_{\partial\mathcal{M}}(\boldsymbol{x},\boldsymbol{\omega}),\boldsymbol{\omega}\right) \\ &+ \int_0^{r_{\partial\mathcal{M}}(\boldsymbol{x},\boldsymbol{\omega})} a\left(\boldsymbol{x},\boldsymbol{x}-r'\boldsymbol{\omega}\right)\sigma_s\left(\boldsymbol{x}-r'\boldsymbol{\omega}\right) \\ &\int_{\mathbb{S}^2} f_p\left(\boldsymbol{x}-r'\boldsymbol{\omega},\boldsymbol{\omega}\cdot\boldsymbol{\psi}\right) G\left(\boldsymbol{x}-r'\boldsymbol{\omega},\boldsymbol{\psi}\right)\,\mathrm{d}\boldsymbol{\psi}\,\mathrm{d}r'. \end{aligned} \tag{27}$$

Comparing Equation (27) with the stationary volume rendering equation (15), we see that they are identical. Therefore, we can identify $L^s(\boldsymbol{x},\boldsymbol{\omega})$ with $G(\boldsymbol{x},\boldsymbol{\omega})$.□

Using Equation (10) from Proposition 1, Equation (3) follows after performing the change of variables $\tau = ct$.

2 Local Similarity Relations in Pathlength-Resolved Case

We prove Lemma 1 of the main paper, restated below for convenience.

Lemma 1. *Let* $\{a_{n,l}(\boldsymbol{x},\tau), n>0, -n\leq l\leq n\}$ *be the coefficients of the spherical-harmonics expansion of the solution* $L(\boldsymbol{x},\boldsymbol{\omega},\tau)$ *of Equation* (4) *at some point* $\boldsymbol{x}\in\mathcal{M}$*, and* $\{f_{p,n}(\boldsymbol{x}), n>0\}$ *the coefficients of the Legendre expansion of* f_p *at that point. If there exists* $N>0$ *such that* $a_{n,l}(\boldsymbol{x},\tau)=0$ *for all* $n>N$*, then two materials* m*,* m^* *will produce equal values* $L(\boldsymbol{x},\boldsymbol{\omega},\tau)$ *if, for* $1\leq n\leq N$*,*

$$\sigma_a(\boldsymbol{x}) = \sigma_a^*(\boldsymbol{x}), \tag{28}$$

$$\sigma_s(\boldsymbol{x})\left(1-f_{p,n}(\boldsymbol{x})\right) = \sigma_s^*(\boldsymbol{x})\left(1-f_{p,n}^*(\boldsymbol{x})\right). \tag{29}$$

Proof. The proof follows easily from Equation (14). The form of this equation is exactly analogous to the stationary RTE of Equation (8), except for replacing $\sigma_a(\boldsymbol{x})$ with $\tilde{\sigma}_a(\boldsymbol{x}, s)$ from Equation (12). We can then directly apply to it the similarity relations derived for the stationary case in [5, 6], to obtain,

$$\sigma_a(\boldsymbol{x}) + \frac{s}{c} = \sigma_a^*(\boldsymbol{x}) + \frac{s}{c^*}, \tag{30}$$

$$\sigma_s(\boldsymbol{x})\left(1 - f_{p,n}(\boldsymbol{x})\right) = \sigma_s^*(\boldsymbol{x})\left(1 - f_{p,n}^*(\boldsymbol{x})\right). \tag{31}$$

If we assume that the two materials have the same index of refraction, and therefore the same speed of light $c = c^*$ in their interior, then Equation (30) reduces to Equation (28). □

Note that, according to Equation (30), in materials with different index of refraction, the local similarity relations for the absorption coefficient σ_a are different in the pathlength-resolved than in the stationary cases. This relates to the fact that, for a fixed value of optical pathlength τ, light will have travelled different (geometric) distances inside the two materials. As a result, the absorption coefficient must change in order for the volumetric attenuation (18) in the two materials to be the same. We do not consider this case in this paper, as we assume that the index of refraction is known.

3 Non-Local Ambiguities in Pathlength-Resolved Case

In this section, we prove Lemma 2 of the main paper. Our proof is based on the formulation of volumetric light transport presented in [2], which discretizes pathlength τ at a resolution h as $\tau = nh, n \in \mathbb{N}$. We summarize that formulation in the form of the following proposition.

Proposition 2. *For any step-size h, we define an n-step path $\bar{\boldsymbol{x}}$ as an ordered sequence of points in the medium $\mathcal{M}$,*

$$\bar{\boldsymbol{x}} = \boldsymbol{x}_0 \xrightarrow{h} \boldsymbol{x}_1 \xrightarrow{h} \ldots \xrightarrow{h} \boldsymbol{x}_n, \tag{32}$$

where $\xrightarrow{h}$ indicates that each segment of the path has length h,

$$\|\boldsymbol{x}_j - \boldsymbol{x}_{j-1}\|_2 = h, \quad \forall j \in \{1, \ldots, n\}. \tag{33}$$

We denote the space of all such paths as $\mathbb{T}_n$. If $h \ll 1/\sigma_t(\boldsymbol{x})$ for all $\boldsymbol{x} \in \mathcal{M}$, then any entry of the light transport matrix $\mathcal{T}_m$ at pathlength $\tau = nh$ can be written as

$$\mathcal{T}_m(\boldsymbol{X}_o, \boldsymbol{X}_i, nh) = \int_{\mathbb{T}_n} \Delta(\bar{\boldsymbol{x}}, \boldsymbol{X}_o, \boldsymbol{X}_i)\, \bar{s}_m(\bar{\boldsymbol{x}})\, \mathrm{d}\bar{\boldsymbol{x}}, \tag{34}$$

where

$$\begin{aligned}\Delta(\bar{\boldsymbol{x}}, \boldsymbol{X}_o, \boldsymbol{X}_i) = &\delta(\boldsymbol{x}(\boldsymbol{X}_i) - o(\bar{\boldsymbol{x}})) \cdot \delta(\boldsymbol{\omega}(\boldsymbol{X}_i) - \boldsymbol{\omega}_o(\bar{\boldsymbol{x}})) \\ &\delta(\boldsymbol{x}(\boldsymbol{X}_o) - e(\bar{\boldsymbol{x}})) \cdot \delta(\boldsymbol{\omega}(\boldsymbol{X}_o) - \boldsymbol{\omega}_e(\bar{\boldsymbol{x}})).\end{aligned} \tag{35}$$

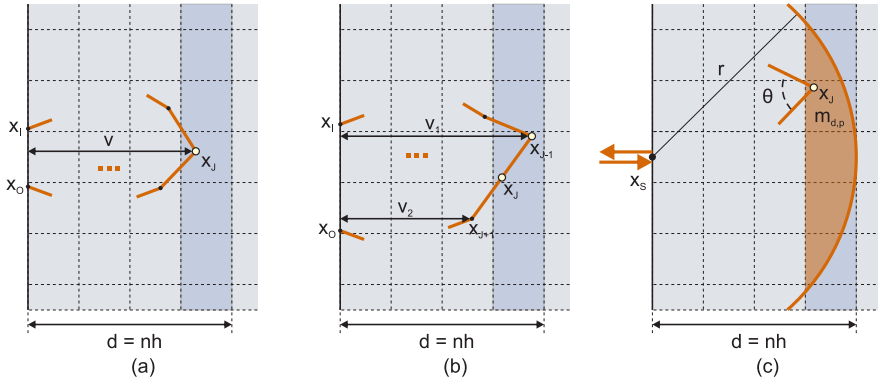

Fig. 1: Schematic for proof of Lemma 2

and the term $\bar{s}_m$ *determines the path's radiance contribution,*

$$\bar{s}_m\left(\bar{\boldsymbol{x}}\right) = \prod_{j=1}^{n-1} s_m\left(\boldsymbol{x}_{j-1} \xrightarrow{h} \boldsymbol{x}_j \xrightarrow{h} \boldsymbol{x}_{j+1}\right), \tag{36}$$

$$s_m\left(\boldsymbol{x}_{j-1} \xrightarrow{h} \boldsymbol{x}_j \xrightarrow{h} \boldsymbol{x}_{j+1}\right) =$$

$$\begin{cases} 1 - h\sigma_t\left(\boldsymbol{x}_{j-1}\right) + h\sigma_s\left(\boldsymbol{x}_{j-1}\right) f_p\left(\boldsymbol{x}_{j-1}, 0\right), & \boldsymbol{\omega}\left(\boldsymbol{x}_{j-1} \xrightarrow{h} \boldsymbol{x}_j\right) = \boldsymbol{\omega}\left(\boldsymbol{x}_j \xrightarrow{h} \boldsymbol{x}_{j+1}\right), \\ h\sigma_s\left(\boldsymbol{x}_{j-1}\right) f_p\left(\boldsymbol{x}_{j-1}, \boldsymbol{\omega}\left(\boldsymbol{x}_{j-1} \xrightarrow{h} \boldsymbol{x}_j\right) \cdot \boldsymbol{\omega}\left(\boldsymbol{x}_j \xrightarrow{h} \boldsymbol{x}_{j+1}\right)\right), & \textit{otherwise.} \end{cases} \tag{37}$$

Intuitively, Proposition 2 provides an alternative path-based formulation for light transport in scattering media. Compared to the formulation used in the main paper (Equation (11) of the main paper), the path integral is over paths consisting of n segments of fixed length h, instead of arbitrary length. At the end of each such segment, a photon will undergo a *propagation event* and will: 1) continue traveling in the same direction (probability $1 - h\sigma_t + h\sigma_s f_p\left(0\right)$); or 2) scatter towards a new direction determined by the local phase function (probability $h\sigma_s$). The length of a path is determined completely by the number of such segments, $\tau\left(\bar{\boldsymbol{x}}\right) = nh$. Therefore, the path sampling function Δ needs only reject paths based on their endpoints, and is not a function of pathlength.

We now use the above proposition to prove Lemma 2 of the main paper, restated below for convenience.

Lemma 2. *Using pathlength decomposition, the configuration of Figure 2(a) of the main paper provides measurements of the form*

$$I_\tau = \begin{cases} Q_\tau + \sum\limits_{p \in k(n)} \sigma_s\left[nh, p\right] \int\limits_0^\pi f_p\left(\left[nh, p\right], \theta\right) R_{\tau,p}\left(\theta\right) \, \mathrm{d}\theta, & \tau = 2nh, \\ S_\tau + \sum\limits_{p \in k(n)} \sigma_t\left[nh, p\right] T_{\tau,p}, & \tau = \left(2n+1\right)h, \end{cases} \tag{38}$$

where Q_τ and $R_{\tau,p}(\theta)$ are functions of material parameters $\{m[d,p], d < nh\}$; and S_τ and $T_{\tau,p}$ of $\{m[d,p], d < nh; \sigma_s[nh,p]; f_p([nh,p],\theta)\}$.

Proof. We prove this lemma in the two-dimensional case for simplicity, with the proof being exactly analogous in the three-dimensional case. We refer to Figure 1 throughout the proof.

From Equations (36)-(37), the radiance contribution of a path will depend on the material parameters of a specific voxel p, d only if the path includes a propagation event at a point inside that voxel.

Consider first a path $\bar{\boldsymbol{x}}$ with endpoints $\boldsymbol{x}_i$, $\boldsymbol{x}_o$ on the material boundary and that includes a propagation event at a point $\boldsymbol{x}_j$ inside the material layer at depth $d = nh$, as shown in Figure 1(a). The distance v of this point from the volume boundary is $v > (n-1)h$. The lengths of the sub-paths $\boldsymbol{x}_i \xrightarrow{h} \ldots \xrightarrow{h} \boldsymbol{x}_j$, $\boldsymbol{x}_j \xrightarrow{h} \ldots \xrightarrow{h} \boldsymbol{x}_o$, are at least equal to v; given that they must be integer multiples of h, we conclude that each of the subpaths must consist of at least n segments. Then, the entire $\bar{\boldsymbol{x}}$ must have at least $2n$ segments. Conversely, given any point $\boldsymbol{x}_j$ inside the material layer at depth $d = nh$, we can always connect it to the material boundary with subpaths of n segments each. Therefore, we have shown that paths $\bar{\boldsymbol{x}}$ with endpoints on the material boundary and that have a propagation event inside voxels at depth $d = nh$ have length $\tau(p) \geq 2nh$.

Consider again a path $\bar{\boldsymbol{x}}$ with endpoints $\boldsymbol{x}_i$, $\boldsymbol{x}_o$ on the material boundary. We now assume that it includes two consecutive propagation events at points $\boldsymbol{x}_{j-1}$, $\boldsymbol{x}_j$ inside the material layer at depth $d = nh$, without a change in direction at $\boldsymbol{x}_j$, and with $\boldsymbol{x}_{j+1}$ being at a layer of depth $d < nh$. This is shown in Figure 1(b). As in the previous case, the distance of $\boldsymbol{x}_{j-1}$ from the boundary is $v_1 > (n-1)h$, and therefore the sub-path $\boldsymbol{x}_i \xrightarrow{h} \ldots \xrightarrow{h} \boldsymbol{x}_{j-1}$ has at least n segments. The distance of $\boldsymbol{x}_{j+1}$ from the boundary is $v_2 > (n-2)h$, and therefore the sub-path $\boldsymbol{x}_j \xrightarrow{h} \ldots \xrightarrow{h} \boldsymbol{x}_o$ has at least $n-1$ segments. Then, together with segments $\boldsymbol{x}_{j-1} \xrightarrow{h} \boldsymbol{x}_j$ and $\boldsymbol{x}_j \xrightarrow{h} \boldsymbol{x}_{j+1}$, the entire $\bar{\boldsymbol{x}}$ must have at least $2n+1$ segments. Conversely, given any points $\boldsymbol{x}_{j-1}, \boldsymbol{x}_j, \boldsymbol{x}_{j+1}$ as above, we can always create a path of $2n+1$ segments with endpoints on the boundary and with $\boldsymbol{x}_{j-1} \xrightarrow{h} \boldsymbol{x}_j \xrightarrow{h} \boldsymbol{x}_{j+1}$ as a subpath. Therefore, we have shown that paths $\bar{\boldsymbol{x}}$ of this kind have length $\tau(p) \geq 2nh$.

Consider now the measurement I_{2nh} captured for pathlength $\tau = 2nh$ from the source-sensor configuration of Figure 1(c). By definition, I_{2nh} will be equal to $\mathcal{T}_m(\boldsymbol{X}_s, \boldsymbol{X}_s, 2nh)$ and therefore, using Equation (34), equal to the sum of radiance contributions from paths $\bar{\boldsymbol{x}} \in \mathbb{T}_{2n}$ with endpoints $\boldsymbol{x}_s$ and appropriate starting and ending directions. All such paths are completely contained inside a circle of center $\boldsymbol{x}_s$ and radius $r = d = nh$. An arc of this circle is shown in Figure 1(c).

From the previous discussion, all paths contributing to I_{2nh} will have at most one propagation event in layer $d = nh$, and no propagation events inside layer $d = (n+1)h$. For paths $\bar{\boldsymbol{x}}$ that have no propagation events inside layer $d = nh$, Equations (36)-(37) imply that their radiance contributions $\bar{s}_m(\bar{\boldsymbol{x}})$ depend only

on material parameters of voxels at smaller depths $d < nh$. If we denote by $B \subset \mathbb{T}_{2n}$ the set of all such paths, then we can define

$$Q_{2nh} = \int_B \Delta\left(\bar{\boldsymbol{x}}, \boldsymbol{X}_o, \boldsymbol{X}_i\right) \bar{s}_m\left(\bar{\boldsymbol{x}}\right) \, \mathrm{d}\bar{\boldsymbol{x}}. \tag{39}$$

Based on the above discussion, Q_{2nh} is a function only of material parameters $\{m\left[d,p\right], d < nh\}$.

For paths $\bar{\boldsymbol{x}}$ that have one propagation event $\boldsymbol{x}_J$ in layer $d = nh$, from Equations (36)-(37) we can write their radiance contributions in the form

$$\begin{aligned}
\bar{s}_m\left(\bar{\boldsymbol{x}}\right) = &\left(\prod_{j=1}^{J-1} s_m\left(\boldsymbol{x}_{j-1} \xrightarrow{h} \boldsymbol{x}_j \xrightarrow{h} \boldsymbol{x}_{j+1}\right)\right) \\
&\cdot h\sigma_s\left[d,p\right] f_p\left(\left[d,p\right],\theta\right) \\
&\cdot \left(\prod_{j=J+1}^{2n-1} s_m\left(\boldsymbol{x}_{j-1} \xrightarrow{h} \boldsymbol{x}_j \xrightarrow{h} \boldsymbol{x}_{j+1}\right)\right) \\
&\triangleq \sigma_s\left[d,p\right] f_p\left(\left[d,p\right],\theta\right) R_{2nh,\bar{\boldsymbol{x}}}.
\end{aligned} \tag{40}$$

where $\{d,p\}$ is the voxel at layer $d = nh$ containing point $\boldsymbol{x}_J$, and θ is the change in direction at that point (see Figure 1(c)). The term $R_{2nh,\bar{\boldsymbol{x}}}$ is a function only of material parameters $\{m\left[d,p\right], d < nh\}$, given that it corresponds to propagation events at voxels of depth $d < nh$. If $C_{\{d,p\},\theta} \subset \mathbb{T}_{2n}$ is the set of all such paths for a specific voxel $\{d,p\}$ and angle θ, then we can write their total radiance contributions as

$$L_{\{d,p\},\theta} = \sigma_s\left[d,p\right] f_p\left(\left[d,p\right],\theta\right) R_{2nh,p}\left(\theta\right) \tag{41}$$

$$R_{2nh,p}\left(\theta\right) \triangleq \int_{C_{\{d,p\},\theta}} R_{2nh,\bar{\boldsymbol{x}}} \, \mathrm{d}\bar{\boldsymbol{x}}. \tag{42}$$

Given that for every voxel $\{d,p\}$ there will be non-empty sets $C_{\{d,p\},\theta} \subset \mathbb{T}_{2n}$ for multiple values θ, we can write the total radiance contributions for all paths with $\boldsymbol{x}_J$ in $\{d,p\}$ as,

$$L_{\{d,p\}} = \int_0^\pi L_{\{d,p\},\theta} \, \mathrm{d}\theta = \sigma_s\left[d,p\right] \int_0^\pi f_p\left(\left[d,p\right],\theta\right) R_{2nh,p}\left(\theta\right) \, \mathrm{d}\theta. \tag{43}$$

The term $L_{\{d,p\},\theta}$ will be non-zero for all values of p for which the voxel intersects with the circle in Figure 1(c). If we denote by $k\left(n\right)$ the set of such values, we can express the contributions of all paths that have one propagation event at layer $d = nh$ as,

$$L_d = \sum_{p \in k(n)} L_{\{d,p\}} = \sum_{p \in k(n)} \sigma_s\left[d,p\right] \int_0^\pi f_p\left(\left[d,p\right],\theta\right) R_{2nh,p}. \tag{44}$$

Finally, we can write the measurement I_{2nh} as the sum of Q_{2nh} and L_d which, using Equations (39) and (44), becomes,

$$I_{2nh} = Q_{2nh} + \sum_{p \in k(n)} \sigma_s \left[d,p\right] \int_0^{\pi} f_p \left(\left[d,p\right],\theta\right) R_{2nh,p}. \tag{45}$$

This is the first part of the desired Equation (38).

The derivation of the second part is similar. At pathlength $\tau = (2n+1)\,h$, the measurement $I_{(2n+1)h}$ includes contributions from four types of paths: 1) paths that have no propagation events in voxels at depth $d = nh$; 2) paths that only have one propagation event in voxels at depth $d = nh$; 3) paths that have two propagation events in voxels at depth $d = nh$, with a change in direction in both events; and 4) paths of the form of Figure 1(b).

The contributions for paths of types 1-3 are included in the term $S_{(2n+1)h}$, which therefore is a function only of material parameters $\{m\left[d,p\right], d < nh\}$ (paths of type 1) and $\{\sigma_s\left[nh,p\right]; f_p\left(\left[nh,p\right],\theta\right)\}$ (paths of type 2 and 3).

Paths of $\bar{\boldsymbol{x}}$ type 4 will have a radiance contribution of the form

$$\begin{aligned}
\bar{s}_m\left(\bar{\boldsymbol{x}}\right) = &\left(\prod_{j=1}^{J-1} s_m\left(\boldsymbol{x}_{j-1} \xrightarrow{h} \boldsymbol{x}_j \xrightarrow{h} \boldsymbol{x}_{j+1}\right)\right) \\
&\cdot \left(1 - h\sigma_t\left[d,p\right] + h\sigma_s\left[d,p\right] f_p\left(\left[d,p\right],0\right)\right) \\
&\cdot \left(\prod_{j=J+1}^{2n-1} s_m\left(\boldsymbol{x}_{j-1} \xrightarrow{h} \boldsymbol{x}_j \xrightarrow{h} \boldsymbol{x}_{j+1}\right)\right) \\
&\triangleq \sigma_t\left[d,p\right] T_{(2n+1)h,\bar{\boldsymbol{x}}} + S_{(2n+1)h,\bar{\boldsymbol{x}}}.
\end{aligned} \tag{46}$$

The terms $S_{(2n+1)h,\bar{\boldsymbol{x}}}$ and $T_{2nh,\bar{\boldsymbol{x}}}\,(2n+1)\,h$ depend only on material parameters $\{m\left[d,p\right], d < nh; \sigma_s\left[nh,p\right]; f_p\left(\left[nh,p\right],\theta\right)\}$. The terms $S_{2nh,\bar{\boldsymbol{x}}}$ are included in $S_{(2n+1)h}$, whereas terms $T_{(2n+1)h,\bar{\boldsymbol{x}}}$ for different paths are accumulated into $T_{(2n+1)h,p}$. By summing over multiple voxels d,p for $d = nh$ and $p \in k\,(n)$, we arrive at the second part of Equation (38). □

4 Initialization

We discuss the two initialization procedures used in Algorithm 1 of the main paper.

Multi-resolution initialization. In this first approach, we begin by assuming that the unknown volume is homogeneous, that is, that there is a single set of material parameters everywhere. Running Algorithm 1 produces a homogeneous material estimate. We then voxelize the volume at progressively higher material resolutions; at each resolution, we rerun Algorithm 1 to recover material parameters at that resolution, using algorithm outpt from the previous resolution as initialization. We repeat this process unti we reach the highest material voxel resolution we consider, 2 mm.

For the original, homogeneous run of Algorithm 1, we initialize the material parameters to $g = 0$ (uniform phase function), $\sigma_a = 0$, and $\sigma_s = 10\,\mathrm{mm}^{-1}$. We use these values to bias the path sampling algorithm towards exploring the entire material volume.

Greedy depth-wise initialization. When using pathlength-decomposed measurements with a frontlighting configuration, as in Figure 2(b) of the main paper, Lemma 2 and the recursive inference argument discussed in Section 4 of the main paper suggest a different way to do initialization. Specifically, starting at $n = 1$ and iteratively at every n, we use Algorithm 1 to process only the measurements at pathlength $\tau = nh$ and to optimize only for the material parameters at voxels of depth $d = \tau/2$ (up to the voxelization resolution). At every iteration, for voxels at lower depths, we fix the material parameters at the values recovered at previous iterations of this recursive procedure. At the end of the recursion, we can use the parameter estimates at every voxel recovered using the above procedure to initialize another run of Algorithm 1, which simultaneously processes all measurements (including measurements from configurations other than frontlighting), and simultaneously optimizes over all material parameters in the volume.

In practice, whenever possible we combine both initialization procedures: At every iteration of the multi-scale procedure, we do material inference at the corresponding resolution using the greedy depth-wise recursive procedure. At every iteration of either the multi-resolution or the greedy depth-wise procedures, we run a few iterations of Algorithm 1, instead of running it until full convergence. In our experiments, we have found that the combined use of these two initialization procedures significantly accelerates convergence.

References

1. Gkioulekas, I., Levin, A., Durand, F., Zickler, T.: Micron-scale light transport decomposition using interferometry. ACM Transactions on Graphics (2015)
2. Gkioulekas, I., Zhao, S., Bala, K., Zickler, T., Levin, A.: Inverse volume rendering with material dictionaries. ACM Transactions on Graphics (2013)
3. Jarabo, A., Marco, J., Muñoz, A., Buisan, R., Jarosz, W., Gutierrez, D.: A Framework for Transient Rendering. ACM Trans. Graph. 33(6), 177:1–177:10 (Nov 2014)
4. O'Toole, M., Heide, F., Xiao, L., Hullin, M.B., Heidrich, W., Kutulakos, K.N.: Temporal Frequency Probing for 5D Transient Analysis of Global Light Transport. ACM Trans. Graph. 33(4), 87:1–87:11 (Jul 2014)
5. Wyman, D., Patterson, M., Wilson, B.: Similarity relations for the interaction parameters in radiation transport. Applied optics 28(24) (1989)
6. Zhao, S., Ramamoorthi, R., Bala, K.: High-order similarity relations in radiative transfer. ACM Transactions on Graphics (2014)